

## Introduction

The High Energy Light Isotope eXperiment (HELIX) (figure 1) is a balloon-borne detector optimized to measure beryllium isotopes ( $Z=4$ ) with an event-by-event mass resolution of 3% [1]. By distinguishing radioactive  $^{10}\text{Be}$  (half-life 1.39 Myr) from stable  $^9\text{Be}$ , HELIX probes Galactic cosmic-ray propagation.

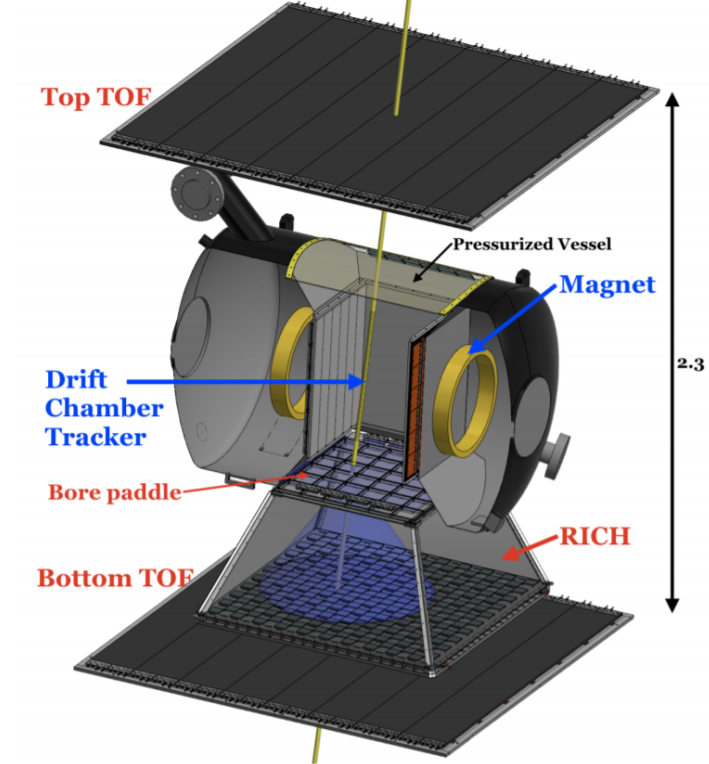


Figure 1. Diagram of HELIX payload [1]

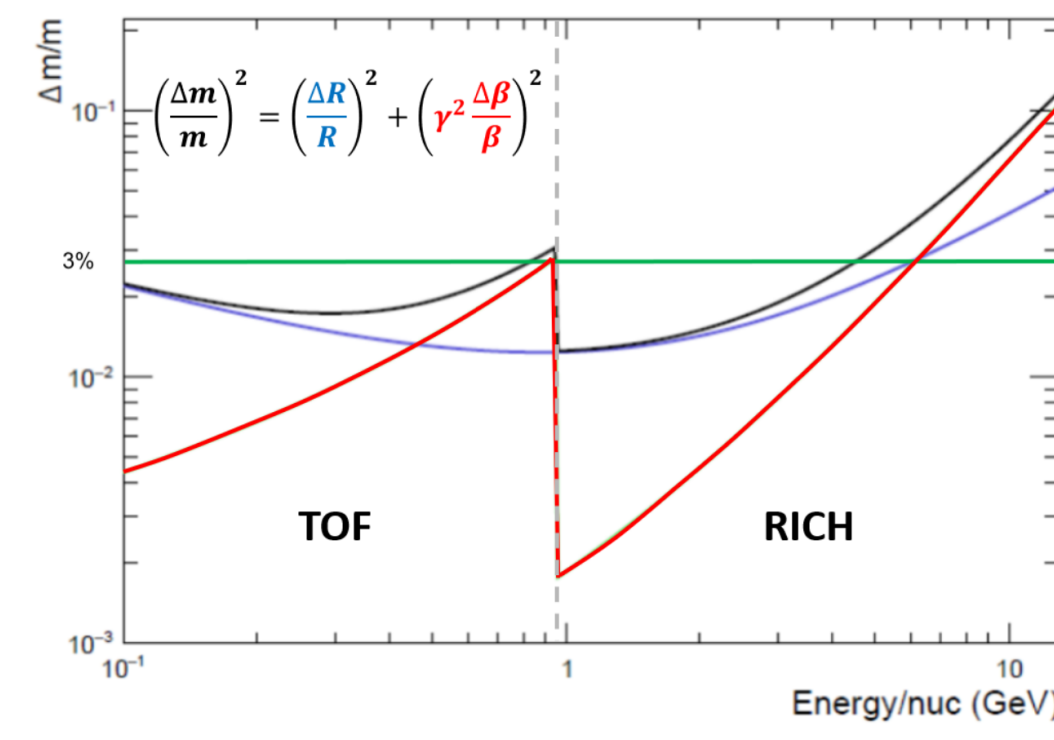


Figure 2. The expected mass resolution for incident  $^{10}\text{Be}$  particles [2]

For velocity measurements above 1 GeV/n, HELIX uses a Ring Imaging Cherenkov (RICH) with aerogel radiators ( $n \sim 1.15$ , 1 cm thick). To achieve the target mass resolution of 3%, a velocity resolution of 0.1% is required (figure 2).

To do this the aerogel radiator's refractive index and thickness must be characterized to the order of  $10^{-4}$  and  $10^{-3}$  [3].

## HELIX flight summary

The first flight of the HELIX experiment launched from the Esrange Space Center near Kiruna, Sweden, on May 28, 2024, lasted 6 d 8 h 27 m (152.5 hours), and the payload landed in Nunavut, Canada. [4].



Figure 3. HELIX flight path, image from [2].

## Ring Imaging Cherenkov Detector (RICH)

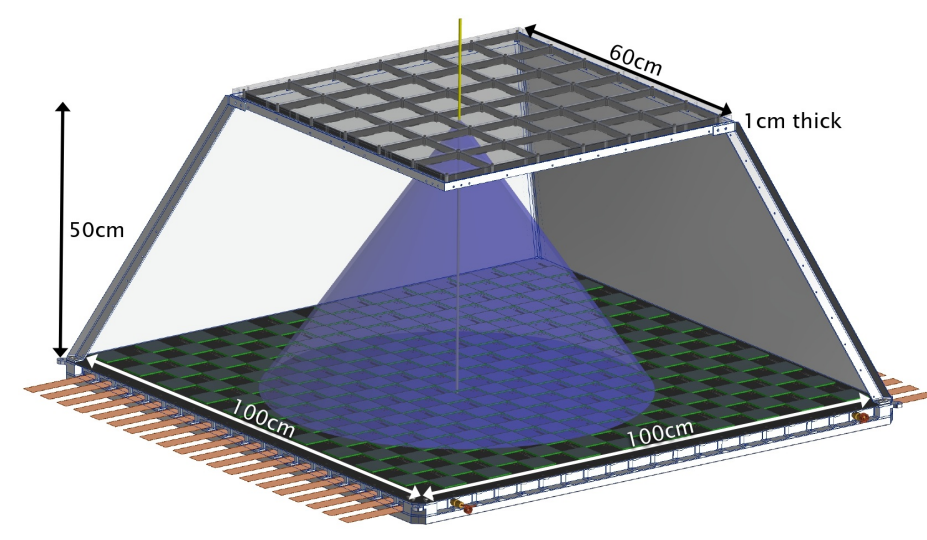


Figure 4. Schematic of RICH with 1 cm thickness aerogel radiator separated by 50 cm from the focal plane where the detectors are located [5].

$$\cos\theta = \frac{1}{n\beta} \quad (1)$$

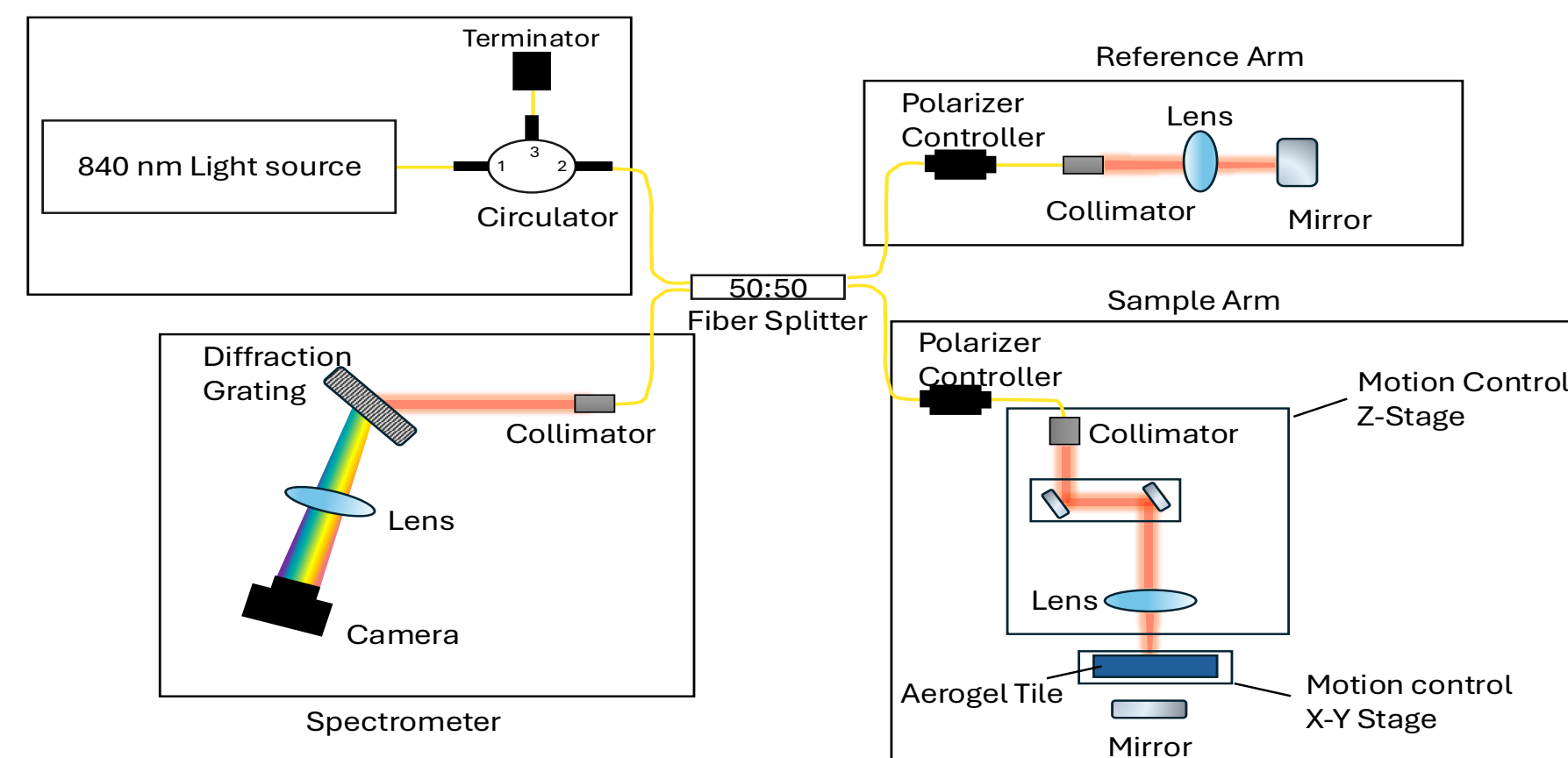
The RICH detector in HELIX is a proximity-focused detector (figure 4). It measures the velocity of particles above 1 GeV/n using Cherenkov radiation (equation 1). It consists of:

- 32 square aerogel tiles ( $10 \times 10 \times 1 \text{ cm}^3$ ) with  $n \sim 1.15$ ,
- 4 NaF tiles with  $n = 1.33$  for TOF-RICH overlap.
- The detector plane consists of 12,800 SiPMs (6 mm  $\times$  6 mm), arranged in 200 arrays of  $8 \times 8$  in a checkerboard pattern

## Spectral Domain Optical Coherence Tomography

SD-OCT is a method based on Michaelson interferometry [6]. SD-OCT can **simultaneously** measure the group refractive index and thickness of aerogel radiators.

1. Light from a broadband source centered at 840 nm, with a bandwidth of 25 nm, splits into a reference arm and sample arm.
2. The light from reference arm and the sample arm interfere and produce an interference pattern.



3. The light combined from the reference arm and sample arm enters the spectrometer. The light disperses from the diffraction grating and the camera records the resulting signal as a spectral interferogram (intensity as a function of wavenumber( $k$ )).

4. The Fourier transform is applied to the spectral interferogram from the wavenumber domain ( $k$ ) to the depth domain ( $Z$ ) (figure 5). The equation to describe the spectral interferogram is:

$$I_D(k) = I_0(k)[R_r^2 + R_s^2 + 2R_r R_s \cos(2kZ)] \quad (2)$$

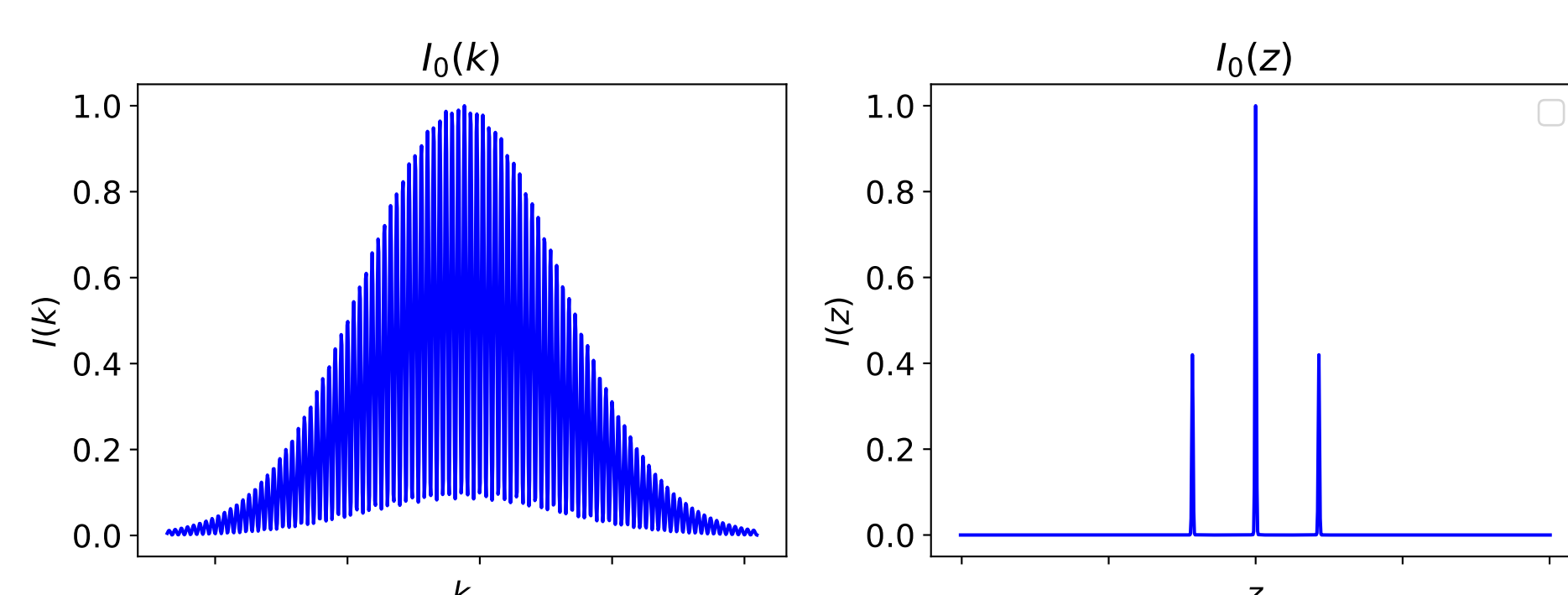


Figure 5. Simulated spectral interferogram for a single interface (left) and its Fourier-transformed depth profile (right). Peaks in the depth profile correspond to the location of reflective surfaces.

## Data Collection Method

$$OPL = n_g \times t \quad (3)$$

The group optical path length (OPL) is the product of a medium's refractive index ( $n_g$ ) and its thickness ( $t$ ).

To determine both values for our aerogel sample, we require two independent measurements (figure 6).

1.  $(Z_{\text{bot}} - Z_{\text{top}}) = n_g t$
2.  $(Z_{\text{mir}_s} - Z_{\text{mir}}) = (n_g - n_{\text{air}})t$

Using these two values, we solve for both  $t$  and  $n_g$ :

$$t = (Z_{\text{bot}} - Z_{\text{top}}) - (Z_{\text{mir}_s} - Z_{\text{mir}}) \quad (4)$$

$$n_g = \frac{Z_{\text{bot}} - Z_{\text{top}}}{t} \quad (5)$$

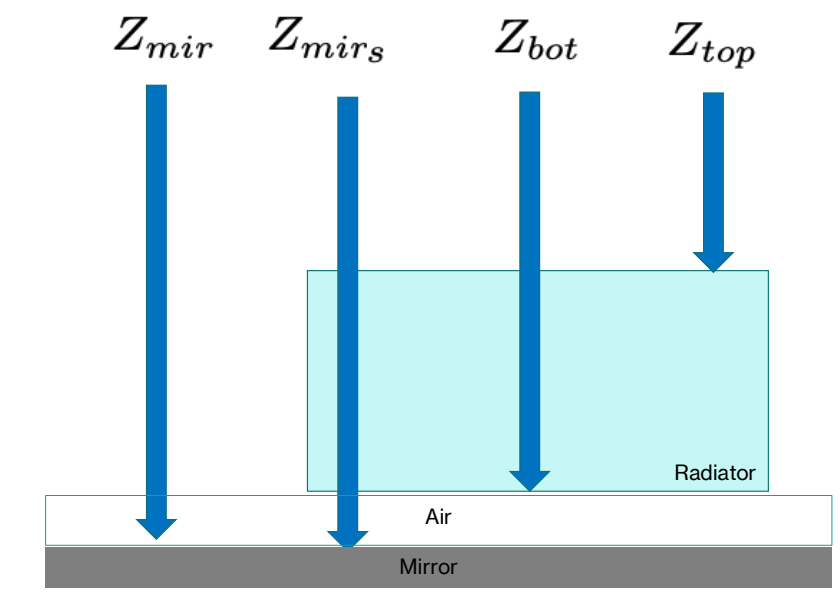


Figure 6. Four measurements are required to extract the thickness and group refractive index of the aerogel tiles. Although the positions are shown across the tile, all measurements must be performed at the same ( $x, y$ ) position on the aerogel tile.

## Results

SD-OCT measures the **group refractive index**, not the phase, because it uses a broadband light source and detects the combined interference from all wavelengths.

The group refractive index of a NaF tile was measured to verify the SD-OCT result against the established literature value (figure 7).

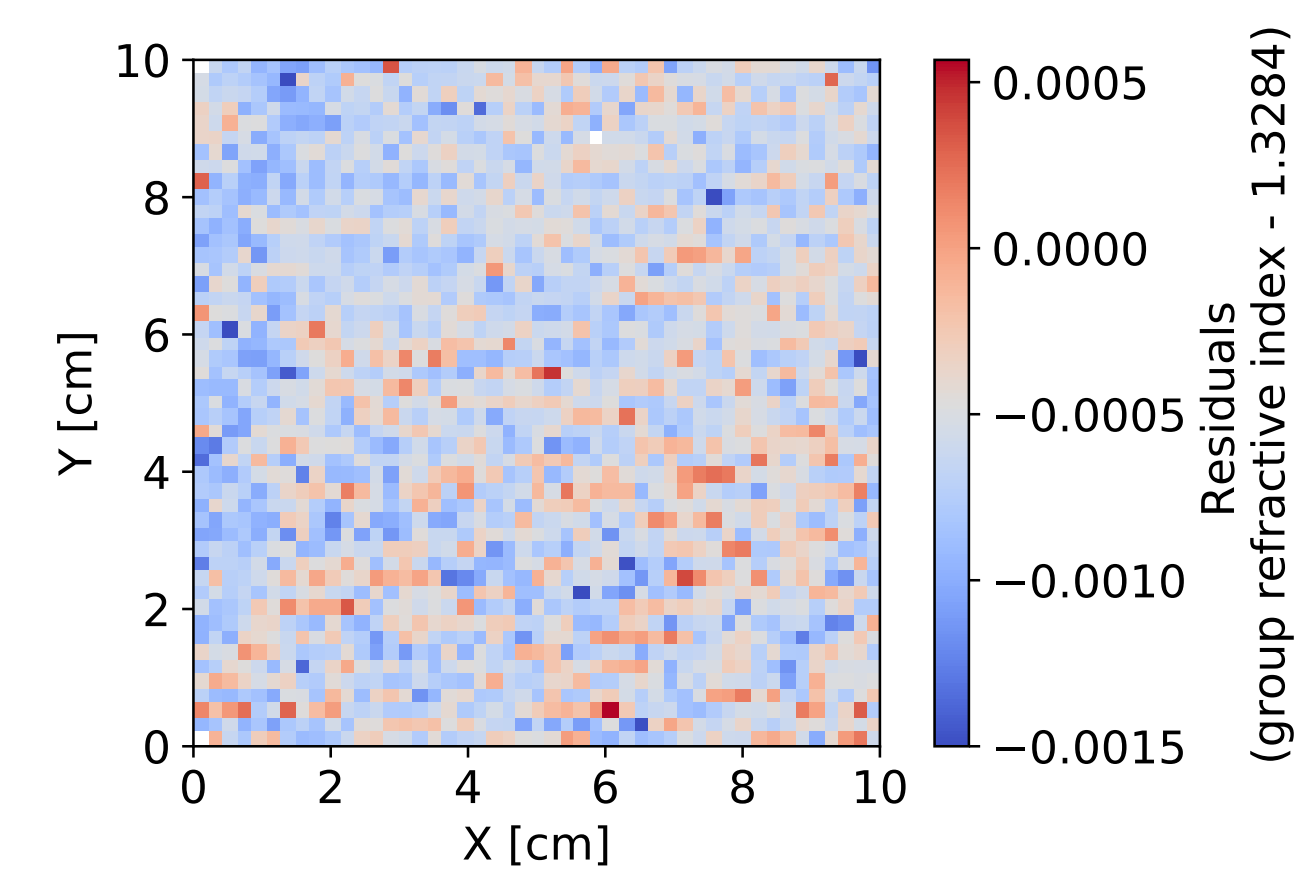


Figure 7. Residual map of NaF tile group refractive index at 840 nm compared with literature reported value from [7].

Four measurements (figure 6) are repeated for each point with a spacing of 2 mm providing a spatially resolved thickness and group index map (Figure 8).

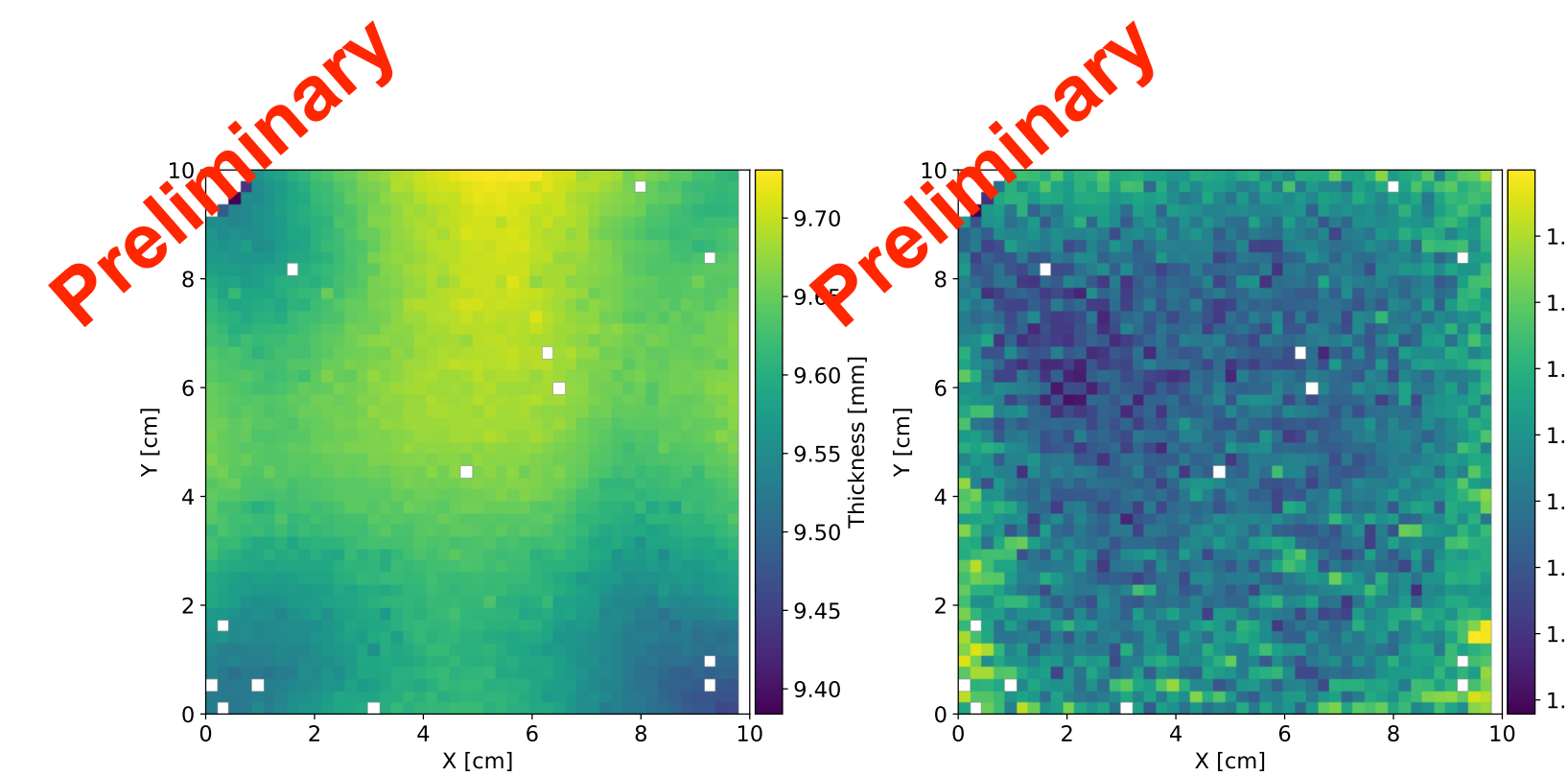


Figure 8. Thickness and group refractive index map of an aerogel tile

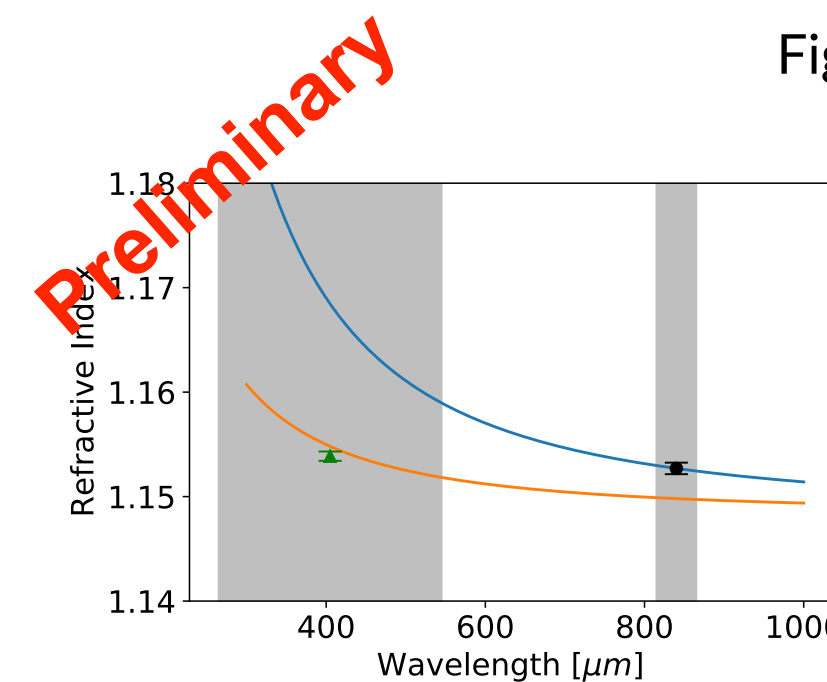


Figure 9. Phase and group refractive equations (orange, blue), compared with OCT group index (black) and electron beam phase refractive index (green) for a single aerogel tile.

The phase refractive index is determined by modeling the aerogel as a composite of silicon dioxide and air.

- Using the Sellmeier equation (refractive index vs. wavelength) and the measured group refractive index, we determine the silicon dioxide content to calculate the phase refractive index (figure 9 – orange curve).

## Conclusion

We demonstrate that SD-OCT can simultaneously characterize the phase refractive index and thickness of aerogel tiles. The estimated uncertainty is 2  $\mu\text{m}$  for thickness and 0.0003 for the phase refractive index. This characterization is critical for accurate Cherenkov angle reconstruction, enabling the HELIX experiment to achieve its target mass resolution for distinguishing isotopes.

## References

- [1] S. Wakely *et al.*, "Cosmic-ray isotope measurements with HELIX," in *Proceedings of 38th International Cosmic Ray Conference—PoS (ICRC2023)*, Sissa Medialab, 2023, p. 118.
- [2] HELIX Collaboration, *HELIX instrument overview*, <http://helix.uchicago.edu/instrument.html>, Accessed: 2025-07-23, 2025.
- [3] P. Allison *et al.*, "Electron-beam calibration of aerogel tiles for the HELIX RICH detector," *Nuclear Instruments and Methods in Physics Research Section A: Accelerators, Spectrometers, Detectors and Associated Equipment*, vol. 1055, p. 168 549, 2023.
- [4] K. McBride *et al.*, *Isotopic composition of cosmic rays with the HELIX balloon project*, Talk presented at the ICRC 2025, Geneva, Switzerland, July 2025, pdf slides: <https://indico.cern.ch/event/1258933/contributions/6481733>, 2025.
- [5] I. Wisher *et al.*, "The Design and Construction of the HELIX RICH Detector," in *36th International Cosmic Ray Conference (ICRC2019)*, vol. 36, 2019, p. 152.
- [6] J. G. Fujimoto and W. Drexler, "Introduction to OCT," in *Optical Coherence Tomography: Technology and Applications*, W. Drexler and J. G. Fujimoto, Eds., Cham: Springer International Publishing, 2015, pp. 3–64, ISBN: 978-3-319-06419-2. DOI: [https://doi.org/10.1007/978-3-319-06419-2\\_1](https://doi.org/10.1007/978-3-319-06419-2_1). [Online]. Available: [https://doi.org/10.1007/978-3-319-06419-2\\_1](https://doi.org/10.1007/978-3-319-06419-2_1).
- [7] M. N. Polianskiy, "Refractive index.info database of optical constants," *Scientific Data*, vol. 11, no. 1, p. 94, Jan. 2024, ISSN: 2052-4463. DOI: [10.1038/s41597-023-02898-2](https://doi.org/10.1038/s41597-023-02898-2). [Online]. Available: <https://doi.org/10.1038/s41597-023-02898-2>.
- [8] M. Tabata *et al.*, "Developing a silica aerogel radiator for the HELIX ring-imaging cherenkov system," *Nuclear Instruments and Methods in Physics Research Section A: Accelerators, Spectrometers, Detectors and Associated Equipment*, vol. 952, p. 161 879, Feb. 2020, ISSN: 0168-9002. DOI: [10.1016/j.nima.2019.02.006](https://doi.org/10.1016/j.nima.2019.02.006). [Online]. Available: <http://dx.doi.org/10.1016/j.nima.2019.02.006>.
- [9] S. R. Uhlhorn, D. Borja, F. Manns, and J.-M. Parel, "Refractive index measurement of the isolated crystalline lens using optical coherence tomography," *Vision Research*, vol. 48, no. 27, pp. 2732–2738, 2008, ISSN: 0042-6989. DOI: <https://doi.org/10.1016/j.visres.2008.09.010>. [Online]. Available: <https://www.sciencedirect.com/science/article/pii/S0042698908004483>.